their volume and density. **All handling** of RI samples was in the dark or in very diffuse light.

Degassing of Solutions. Known volumes of neat MeI or EtI or Fe solutions of appropriate concentrations were syringed into sidearms equipped with break seals and degassed by 11-14 freeze-pump-thaw cycles to stick vacuum ($<10^{-5}$ (mmHg)).[45] Degassed sidearms wrapped with aluminum foil were connected to the main body of the flash cell which included the cylindrical flash cell (l = 15.0 cm) filled at the ends with Pyrex flats, a degassing bulb, and a calibrated UV cell for monitoring the anthracene concentrations of degassed solutions. The flash cell system was then cleaned by rinsing several times with distilled acetone, drying under reduced pressure, rinsing with the solvent employed in the experiment, and repeating the drying procedure. Exactly 40 mL of anthracene solution was syringed into the degassing bulb which contained a stainless steel bullet for breaking the break seal(s). Benzene solutions required at least 11 freeze-pump-thaw cycles for thorough degassing while methylcyclohexane solutions required 12-13 cycles.

Transient Measurements. The flash spectroscopy apparatus was that previously described.[10,11] A 6-nm band-pass at $^1/_2$ intensity was employed on the monochromator.[10] The light of the two air-discharge flash lamps was filtered with a solution (13.5 g of $CuSO_4 \cdot 5H_2O$, 27.5 mL of NH_4OH to 250 mL with H_2O, 1 cm path length) having <1% transmittance at $\lambda < 373$ nm and maximum transmittance at 424 nm for all runs except 1j, 1k, 2a, 2b, and 2c for which a more dilute filter solution was employed having <1% transmittance at $\lambda < 358$ nm. The monitoring beam was filtered through a 1 cm path length solution (27.1 g of $CuSO_4 \cdot 5H_2O$, 30.2 g of $NaNO_2$, and 50 mL of NH_4OH to 1 L with H_2O) having 1% transmittance at $\lambda < 400$ nm, except for runs 1j, 1k, 2a, 2b, and 2c for which a more dilute filter solution was employed which transmitted light of $\lambda > 346$ nm. The transient signals were monitored at 429 nm for benzene and at 421 nm for methylcyclohexane solutions. After 2-4 $^3A^*$ decay curves were recorded, a portion of the solution was transferred to the UV sidearm and the UV absorbance obtained (Perkin-Elmer λ5). The break seal was then broken, uniform solution was attained by shaking, and the procedure was repeated. In the Fe/EtI experiment the Fe sidearm break seal was always broken first. With RI, data were collected within the first 10 flashes for extrapolation to the $k_{1,0}'$ values.

Concentrations. Anthracene concentrations were based on absorbances in the side cells with use of the following molar absorptivities (λ, nm; ε, M^{-1} cm^{-1}): (378.6; 7.94×10^3), (359.1; 8.49×10^3), (368.2; 2.16×10^3), (349.2; 3.10×10^3) in benzene, and (375.6; 8.42×10^3), (356.4; 8.65×10^3) in methylcyclohexane. Small corrections for the absorbance of MeI and EtI were applied (λ; ε): (378.6; 1×10^{-3}), (368.2; 5×10^{-3}), (359.2; 1.7×10^{-2}) for MeI in benzene, and (375.5; 4×10^{-3}), (356.4; 4×10^{-2}) for EtI in methylcyclohexane. Fe (2×10^{-7} M) does not contribute at the monitoring λ's. No changes in the ε values of A were noted in the presence of 1.08 M MeI in benzene.

Concentrations of MeI and EtI were determined by GLC with use of EtI as internal standard for MeI and vice versa. A DB-5 fused silica capillary column (30 m × 0.32 mm OD) was employed in a Varian-Aerograph Model 2700 instrument and a Hewlett Packard 3390A electronic integrator. Concentrations determined in this way checked closely with those expected from RI volumes and densities.[46]

Acknowledgement is made to the donors of The Petroleum Research Fund, administered by the American Chemical Society, for partial support of this research. This research was also supported by NSF Grant CHE 84-00706.

(45) Initial experiments in which MeI and EtI in benzene and methylcyclohexane solutions were degassed in the sidearms generally gave higher apparent quenching constants.

(46) **Note Added in Proof:** The analysis of k_2 has recently been refined[47] to account for two nearly cancelling errors: (a) the model reaction on which k_{dif} was based is an A + B reaction for which $k_{obsd} \simeq (1/2)k_{dif}^{AB}$; (b) TTA is an A + A reaction for which $k_a = k_{dif}^{AA} = (1/2)k_{dif}^{AB}$. This refinement does not significantly affect the conclusions in this paper.

(47) Saltiel, J.; Atwater, B. W. *Adv. Photochem.*, submitted.

Spectroscopic Studies of the Binuclear Ferrous Active Site of Deoxyhemerythrin: Coordination Number and Probable Bridging Ligands for the Native and Ligand Bound Forms

Richard C. Reem and Edward I. Solomon*

Contribution from the Department of Chemistry, Stanford University, Stanford, California 94305. *Received May 29, 1986*

Abstract: The binuclear Fe(II) active site of deoxyhemerythrin (deoxyHr) was studied using absorbance, circular dichroism (CD), variable-temperature magnetic circular dichroism (MCD), and EPR spectroscopies. CD studies show the native deoxyHr site contains one five-coordinate and one six-coordinate ferrous iron. In addition N_3^-, OCN^-, and F^- were found to bind to the active site, producing large spectral changes best explained as the binding of a single anion to the five-coordinate iron, yielding two six-coordinate Fe(II)s. No other anions were found to bind. The variable-temperature MCD data were interpreted by fitting the data to energies and g values of low-lying binuclear ferrous ground states, predicted by calculations employing the spin Hamiltonian containing both exchange coupling ($\mathcal{H} = -2JS_1 \cdot S_2$) and single-site zero field splitting (ZFS). The native deoxyHr data showed the Fe(II) to be antiferromagnetically coupled with $-J \sim 12$-38 cm^{-1}, which indicates the irons are likely bridged by hydroxide. The ligand bound forms all show weak ferromagnetic coupling, indicating the OH superexchange pathway is perturbed significantly. The binding of anions apparently changes the charge density of the iron, raising the pK_a of the bridge, and likely results in protonation of the hydroxide. Further, the intensity mechanism of an interesting $g_\parallel \sim 16$ EPR signal originating from the $|4,\pm4\rangle$ ground state in the deoxyN_3^-Hr species is analyzed. Finally, these results on exogenous ligand binding and endogenous ligand bridging at the binuclear Fe(II) site of Hr are correlated to the protein reactivity.

Hemerythrin (Hr) is a binuclear, non-heme iron protein, which serves as the oxygen-carrying protein in four phyla of marine organisms.[1] Most of these are octameric and bind dioxygen noncooperatively, although the Hrs from at least some brachiopods[2] do bind dioxygen cooperatively. Hemerythrin exists in two physiologically important forms: oxyhemerythrin, having two ferric irons with peroxide bound end-on to only one iron, and

(1) (a) Okamura, M. Y.; Klotz, I. M. *Inorganic Biochemistry*; Eichhorn, G. L., Ed.; Elsevier: New York, 1973; pp 320-343. (b) Kurtz, D. M., Jr.; Shriver, D. F.; Klotz, I. M. *Coord. Chem. Rev.* **1977**, *24*, 145-178. (c) Klippenstein, G. L. *Am. Zool.* **1980**, *20*, 39-51.

(2) (a) Manwell, C. *Science (Washington, D.C.)* **1960**, *132*, 550. (b) Richardson, D. E.; Reem, R. C.; Solomon, E. I. *J. Am. Chem. Soc.* **1983**, *105*, 7780-7781.

0002-7863/87/1509-1216$01.50/0

deoxyhemerythrin, in which the dioxygen molecule has been removed, leaving the irons in the ferrous oxidation state. Much insight into this active site has derived from studies of the stable but nonphysiological met derivatives, where both irons are Fe(III). Due to crystallographic and spectroscopic studies, the structure of these forms is well-known. Crystal structures have shown[3] that the metN_3^- species contains two hexacoordinate irons bridged by an oxide and two carboxylate ligands. In addition, one iron has three histidine ligands and the other has two histidines and the bound azide. The structure of the met"aquo" form[3a] shows no bound exogenous ligand, with one iron being pentacoordinate. Previously, Mössbauer[4] studies had shown that both irons in the met forms, and in oxyhemerythrin as well, are high spin ferric. In addition magnetic susceptibility[5] and optical absorbance[6] showed the two irons are joined by an oxo bridge. Finally, single crystal polarized absorbance[7] showed that azide is bound end-on, to only one iron, and peroxide is bound similarly in oxyHr.

Resonance Raman spectroscopy[8] first showed that oxygen is bound asymmetrically, as peroxide, and has recently[9] shown that this is most likely hydroperoxide. Recent X-ray crystallographic difference electron density maps[10] also indicate that oxyHr has a structure very similar to metN_3^-, with the peroxide replacing the azide.

The deoxy form has been much less studied and is less understood. Early Mössbauer work clearly demonstrated that both irons are high spin ferrous,[4] and spectra showing electronic transitions in the near-IR[11] were interpreted as indicating the iron is present as roughly octahedral Fe(II). In a recent preliminary report we have shown, using MCD, CD, and EPR, that the irons are five and six coordinate and are bridged by a hydroxo bridge.[12] Finally, a low-resolution X-ray difference map[10] suggests the coordination of the irons to be similar to that in metaquo, with one five- and one six-coordinate iron. In this study we use EPR and CD and MCD studies of the Fe(II) ligand field transitions to probe in more detail the deoxyhemerythrin active site and its ligand bound forms, in order to gain insight into the physiological mechanism of the protein.

The high-spin ferrous free ion has a ^5D ground state, which splits into $^5T_{2g}$ and ^5E_g states in a cubic ligand field. In the octahedral case, the triply degenerate state is the ground state with the ^5E_g state $10D_q$ to higher energy. This is the only spin-allowed ligand field transition and is usually seen as a weak band at about 10000 cm^{-1}. In actuality the ^5E state is always split, either by an excited-state Jahn–Teller distortion or more often by a static low-symmetry distortion in the ground state, resulting in a pair of absorption peaks split by 1000–2000 cm^{-1}, which is the signature of six-coordinate ferrous iron.[13] Spin-forbidden transitions occur at higher energies[14] but are very weak and generally have not been interpreted. In tetrahedral geometry, the same two states arise, but since $D_{q_{tet}} \sim -^4/_9 D_{q_{oct}}$, the ^5E state is the ground state, and a broad d–d transition is observed[15] near 3000–5000 cm^{-1}. Pentacoordinate complexes have lower symmetry, thereby splitting the orbital E and T_2 degeneracies, and give a ligand field strength intermediate to that of the four- and six-coordinate complexes. Electronic spectra taken on a range of five-coordinate complexes[16] show single bands near 10000 cm^{-1} and near 5000 cm^{-1} or lower in most of the complexes. These can thus be distinguished from tetrahedral coordination by the presence of one high-energy band and from low-symmetry split six-coordinate spectra by the low energy of the 5000-cm^{-1} transition and the low total ligand field strength.

Most ferrous complexes are of low enough symmetry that the ground state is orbitally nondegenerate, leaving the 5-fold spin degeneracy of the $S = 2$ ion. In the presence of only an axial distortion, second-order spin–orbit coupling with the orbital excited states causes the spin quintet to split into $M_s = \pm 2$ and $M_s = \pm 1$ doublets, with energies $4D$ and D, respectively, and the $M_s = 0$ singlet, with energy set at zero.[17] With an axial compression the axial zero field splitting (ZFS) parameter D is positive, resulting in the $M_s = 0$ ground state, while the $M_s = \pm 2$ doublet is the ground state for axial elongation.[18] At very low temperatures, magnetic susceptibility, EPR, or MCD studies can distinguish these cases and can be fit to give the value of D. This can be as large as about 15 cm^{-1} in nearly octahedral ferrous iron complexes[19] but is smaller with increased low-symmetry distortion. Since this is an integer spin system, the remaining degeneracy is completely removed in lower than axial symmetry, which along with rapid relaxation is responsible for the general lack of Fe(II) EPR signals.

In a binuclear ferrous system such as hemerythrin, the $S = 2$ irons can interact to give five levels split by exchange coupling. These levels, designated by their total spin $S_T = 0$, 1, 2, 3, and 4, are split by energies of 2-, 4-, 6-, and $8J$, respectively, and have degenercies of $2S_T + 1$. If the exchange coupling constant J is negative, the coupling is antiferromagnetic, yielding the singlet ground state, whereas ferromagnetic coupling gives the $S_T = 4$ ground state and $J > 0$. J is known to range from $\sim +1$ to -14 cm^{-1} for Fe(II)[20] and by comparison with other metals (vide infra) could be as large as -100 cm^{-1} with the proper ligand set. In cases where J is much larger or smaller than D, exchange coupling or ZFS will dominate and the system can be treated as the limiting binuclear or mononuclear case, with the smaller term being merely a perturbation. However, when the two effects are of comparable magnitude, a complicated energy level arrangement arises.[21] This situation will be treated in the Analysis section.

One technique emphasized in this study is the use of the temperature dependence of the magnetic circular dichroism (MCD) spectrum to examine the magnetic properties of the ground state. MCD signals which show large temperature dependence are called C terms and arise due to transitions from a degenerate electronic ground state which splits in a magnetic field.[22]

In systems containing an isolated doublet ground state, one can plot the signal intensity of an MCD peak, against H/T, and all

(3) (a) Stenkamp, R. E.; Sieker, L. C.; Jensen, L. H. *J. Am. Chem. Soc.* **1984**, *106*, 618–622. (b) Sheriff, S.; Hendrickson, W. A.; Smith, J. L. *Life Chem. Rep.* **1983**, *1*, 305–308.

(4) (a) Okamura, M. Y.; Klotz, I. M.; Johnson, C. E.; Winter, M. R. C.; Williams, R. J. P. *Biochemistry* **1969**, *8*, 1951–1958. (b) Clark, P. E.; Webb, J. *Biochemistry* **1981**, *20*, 4628–4632.

(5) (a) Moss, T. H.; Moleski, C.; York, J. L. *Biochemistry* **1971**, *10*, 840–842. (b) Dawson, J. W.; Gray, H. B.; Hoenig, H. E.; Rossman, G. R.; Schredder, J. M.; Wang, R.-H. *Biochemistry* **1972**, *11*, 461–465.

(6) Garbett, K.; Darnall, D. W.; Klotz, I. M.; Williams, R. J. P. *Arch. Biochem. Biophys.* **1969**, *135*, 419–434.

(7) Gay, R. R.; Solomon, E. I. *J. Am. Chem. Soc.* **1978**, *100*, 1972–1973.

(8) (a) Dunn, J. B. R.; Shriver, D. R.; Klotz, I. M. *Proc. Natl. Acad. Sci. U.S.A.* **1973**, *70*, 2582–2584. (b) Kurtz, D. M., Jr.; Shriver, D. R.; Klotz, I. M. *J. Am. Chem. Soc.* **1976**, *98*, 5033–5035.

(9) Shiemke, A. K.; Loehr, T. M; Sanders-Loehr, J. *J. Am. Chem. Soc.* **1986**, *108*, 2437–2443.

(10) Stenkamp, R. E.; Sieker, L. C.; Jensen, L. H.; McCallum, J. D.; Sanders-Loehr, J. *Proc. Natl. Acad. Sci. U.S.A.* **1985**, *82*, 713–716.

(11) Loehr, J. S.; Loehr, T. M.; Mauk, A. G.; Gray, H. B. *J. Am. Chem. Soc.* **1986**, *102*, 6992–6996.

(12) Reem, R. C.; Solomon, E. I. *J. Am. Chem. Soc.* **1984**, *106*, 8323–8325.

(13) (a) Nicholls, D. *The Chemistry of Iron, Cobalt and Nickel*; Pergamon: New York, 1973; pp 979–1051. (b) Little, B. F.; Long, G. J. *Inorg. Chem.* **1978**, *17*, 3401–3413.

(14) Pollini, I.; Spinolo, G.; Benedek, G. *Phys. Rev. B* **1980**, *22*, 6369–6390.

(15) Forster, D.; Goodgame, D. M. L. *J. Chem. Soc.* **1965**, 454–458.

(16) (a) Ciampolini, M.; Speroni, G. P. *Inorg. Chem.* **1966**, *5*, 45–49. (b) Ciampolini, M.; Nardi, N. *Inorg. Chem.* **1966**, *5*, 1150–1154. (c) Riley, D. P.; Merrell, P. H.; Stone, J. A.; Busch, D. H. *Inorg. Chem.* **1975**, *14*, 490–494. (d) Merrell, P. H.; Goedken, V. L.; Busch, D. H. *J. Am. Chem. Soc.* **1970**, *92*, 7590–7591. (e) Reiff, W. M.; Erickson, N. E.; Baker, W. A., Jr. *Inorg. Chem.* **1969**, *8*, 2019–2021.

(17) Abragam, A.; Bleaney, B. *Electron Paramagnetic Resonance of Transition Ions*; Clarendon: Oxford, 1970.

(18) Gill, J. C.; Ivey, P. A. *J. Phys. C.: Solid State Phys.* **1974**, *7*, 1536–1550.

(19) (a) Rudowicz, C. *Acta Phys. Pol.* **1975**, *A47*, 305–321. (b) Champion, P. M.; Sievers, A. J. *J. Chem. Phys.* **1977**, *66*, 1819–1825.

(20) (a) Spiro, C. L.; Lambert, S. L.; Smith, T. J.; Duesler, E. N.; Gagnē, R. R.; Hendrickson, D. N. *Inorg. Chem.* **1981**, *20*, 1229–1237. (b) Lambert, S. L.; Hendrickson, D. N. *Inorg. Chem.* **1979**, *18*, 2683–2686. (c) Long, G. L. *Inorg. Chem.* **1978**, *17*, 2702–2707.

(21) Kennedy, B. J.; Murray, K. S. *Inorg. Chem.* **1985**, *24*, 1552–1557.

(22) Stephens, P. J. *Adv. Chem. Phys.* **1976**, *35*, 197–264.

points fall on a single curve.[23] This can be used to extract information on the rate of saturation and therefore on the effective g value of the ground state, even when EPR spectra cannot be obtained, as is usually the case for ferrous complexes. In addition, when thermally accessible excited states are present, the data points obtained at different temperatures do not lie on the same curve but rather form a set of nested curves.[24] Analysis of these curves, in favorable circumstances, can yield the energy and g value of these low-lying excited states. Finally, if the ground doublet is split in zero field, a pseudo-C term results, which can also give a nested set of saturation curves.[25] This yields information on the rhombic splitting of the ground-state non-Kramers doublet.

Using temperature-dependent MCD to study the binuclear ferrous active site of deoxyhemerythrin allows us to separate the contributions that zero field splitting and exchange coupling make to the ground-state splitting. This is done by determining the degeneracy and the g value of the ground state and the energy and character of the lowest lying excited states. The D and J values thus obtained relate to the geometry of each iron site and the coupling between the two irons due to bridging ligands that are present. The combination of the analysis of the ligand field transitions and the magnetic properties of the ground state from EPR and MCD allows us to evaluate structural models for the deoxyhemerythrin active site and its ligand bound forms and correlate these with reactivity.

Experimental Section

Oxyhemerythrin was obtained from the coelomic fluid of the sipunculid *Phascolopsis gouldit*, which were purchased live from Marine Biological Laboratories, Woods Hole, MA. After standard purification of the protein,[26] it was dialyzed against 0.1 M Tris·SO_4^{2-}, pH 7.7. DeoxyHr was prepared by dialyzing oxy against 5 mM $Na_2S_2O_4$ at least 12 h and subsequently dialyzing against buffer to remove excess dithionite. Deoxygenated nitrogen was bubbled through the buffer to keep the system anaerobic. The protein concentration is expressed as the monomer concentration and was determined spectroscopically, first by using the 500-nm transition in oxy and 446-nm transition in metN_3^-Hr[6] and second from the CD by using the $\Delta\epsilon$ values listed in the Results section.

For the measurement of the binding constants, a 1-mL sample of approximately 2 mM deoxyHr was injected into a cell previously sealed with a septum and deoxygenated. Changes were measured in the CD spectrum upon small additions of concentrated (~5 M) anion solutions. The data were plotted as a Skatchard plot, giving a straight line for the complete titration. The many anions which did not bind were found to give no change in the spectrum, even up to 0.5 M. At most only minimal denaturation occurred at even the highest anion concentrations. Excess dithionite did not affect the binding experiments. All titrations were carried out on a JASCO J500C spectrophotometer with a S1 photomultiplier tube.

The near-IR absorbance spectra were measured on a Cary 17 instrument. The water in the sample was exchanged with D_2O by repeated concentration (5×) with an Amicon ultrafiltration cell with PM10 membrane and subsequent dilution with pD 8.1, 0.1 M Tris·SO_4^{2-}·D_2O buffer. The sample was finally concentrated to 20 mM and reduced with dithionite (0.3 M in D_2O). The sample had previously been reduced and exposed to air to minimize the amount of met present. The deoxy spectrum was measured against buffer in the reference beam. The deoxyN_3^- sample was treated analogously, with 0.2 M NaN_3 present, and also measured with deoxy + Cl^- (0.2 M) in the reference beam. The near-IR CD spectra were run using the same samples in our laboratory (down to 1100 nm) and in Prof. Philip Stephens' laboratory at the University of Southern California (1100–1900 nm).

The MCD samples were made by adding glycerol to the sample for glassing purposes, to give 60% glycerol by volume. For the deoxyHr spectrum, addition of NaCl or $NaClO_4$ (0.2 M final concentration) was found to produce much better glasses and thus higher quality data,

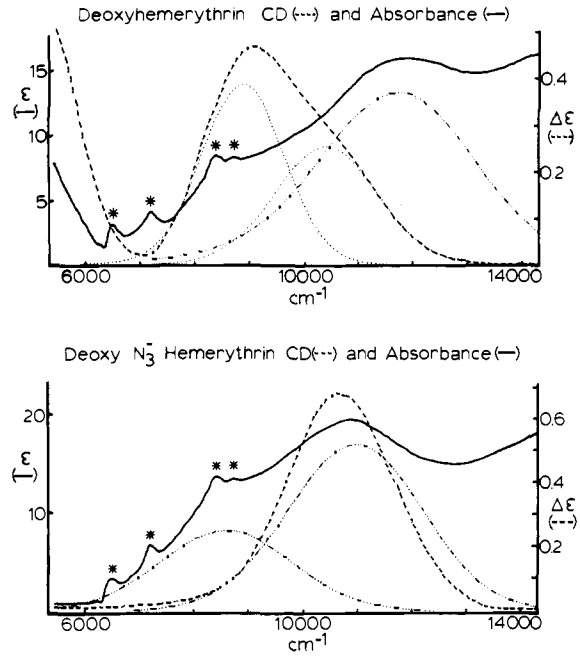

Figure 1. Room-temperature absorbance (—) and circular dichroism (---) spectra for deoxyhemerythrin (a, top) and azidodeoxyhemerythrin (b, bottom). The sharp absorbance features (*) arise from vibrational overtones from the protein backbone, and the rising absorbance toward the UV is due to a small (~2%) impurity of methemerythrin. The three transitions in the 10 000-cm^{-1} region are shown by Gaussian resolution of the CD (···) and absorbance (-···-) spectra.

without perturbing the shape, position, or intensity of the transitions. Addition of Cl^- to the deoxyN_3^-Hr solution also produced no changes.

The MCD sample holder consisted of two quartz disks separated by a 3-mm rubber O-ring spacer. The sample was injected through the spacer and placed into the Oxford SM4-6T magnet system. The optical density was obtained from the θ of the CD features. The spectra were measured on a JASCO J500C spectropolarimeter with an enlarged sample compartment and magnetically shielded PM tube, as previously described.[27]

EPR spectra were measured on a Bruker ER 220D-SRC equipped with an Oxford pumped helium cryostat. Samples were prepared anaerobically, placed into EPR tubes, and quickly frozen in liquid nitrogen until placed into the cryostat.

Results

CD. Figure 1 shows the CD and electronic absorption spectra for deoxyhemerythrin, from near 5000 cm^{-1} (the D_2O cutoff) to 14 000 cm^{-1}. The CD spectrum shows an asymmetrical feature near 10 000 cm^{-1}, which can be resolved into two bands at 8760 cm^{-1} ($\Delta\epsilon$ = 0.38 cm^{-1} M^{-1}) and 10 350 cm^{-1} ($\Delta\epsilon$ = 0.25 cm^{-1} M^{-1}), and an additional feature near 5000 cm^{-1} ($\Delta\epsilon$ = 0.5–1.0 cm^{-1} M^{-1}). When cooled to 77 K the CD features increase about 40% in intensity but band shapes and peak positions remain approximately constant. The absorbance spectrum shows a well-defined peak at 11 600 cm^{-1} (ϵ = 10–15 cm^{-1} M^{-1}) which is clearly not observed in the CD. In addition there is a shoulder at 8770 cm^{-1} (ϵ ~ 6 cm^{-1} M^{-1}) and the high-energy tail of a peak[28] at about 5000 cm^{-1} (ϵ ~ 6–10 cm^{-1} M^{-1}) which are seen at the same energy in the CD spectrum. Therefore, there are at least four IR ligand field transitions in deoxyHr. No further transitions are visible until the protein absorbance above 300 nm.

The CD and absorption spectra remain unchanged upon anaerobic addition of ClO_4^-, Cl^-, Br^-, I^-, CN^-, NCN^{2-}, and NCS^-, at anion concentrations up to 0.5 M. There is also no apparent change in the spectra with pH over the stable range of the protein (pH 5.5–9.0). However, upon the addition of N_3^-, OCN^-, or F^-,

(23) (a) Schatz, P. N.; Mowery, R. L.; Krausz, E. R. *Mol. Phys.* **1978**, *35*, 1537–1557. (b) Johnson, M. K.; Thomson, A. J.; Robinson, A. E.; Rao, K. K.; Hall, D. O. *Biochem. Biophys. Acta* **1981**, *667*, 433–451. (c) Browett, W. R.; Fucaloro, A. F.; Morgan, T. V.; Stephens, P. J. *J. Am. Chem. Soc.* **1983**, *105*, 1868–1872.

(24) Thomson, A. J.; Johnson, M. K. *Biochem. J.* **1980**, *191*, 411–420.

(25) Whittaker, J. W.; Solomon, E. I. *J. Am. Chem. Soc.* **1986**, *108*, 835–836.

(26) Klotz, I. M.; Klotz, T. A.; Fiess, J. A. *Arch. Biochem. Biophys.* **1957**, *68*, 284–299.

(27) Allendorf, M. D.; Spira, D. J.; Solomon, E. I. *Proc. Natl. Acad. Sci. U.S.A.* **1985**, *82*, 3063–3067.

(28) The 5000-cm^{-1} absorption peak is seen only by difference spectra, in comparison with azidodeoxyhemerythrin.

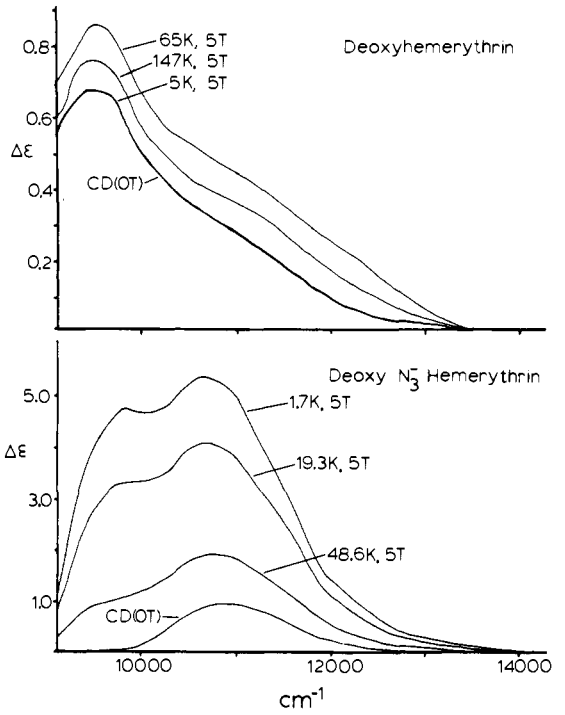

Figure 2. Magnetic circular dichroism (MCD) of deoxyhemerythrin (top) in 0.1 M, pH 7.7 Tris·SO_4 buffer in 60% glycerol/0.2 M NaCl glass and azidodeoxyhemerythrin (bottom), same conditions with NaN_3 replacing NaCl. For deoxyHr the zero field base line and 5 K, 5-T MCD spectrum are coincident lines as labeled. Notice the maximum MCD intensity is achieved near 65 K. Below, the most intense deoxyN_3^- signal is obtained at the lowest temperature. Note scale change between top and bottom spectra.

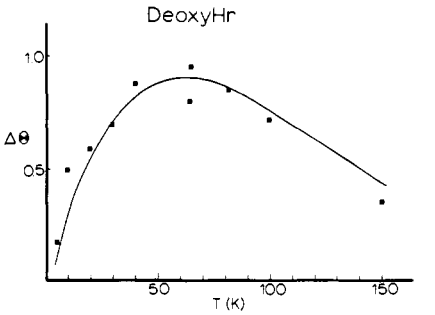

Figure 3. Temperature dependence of deoxyhemerythrin MCD intensity. Experimental conditions are listed under Figure 2.

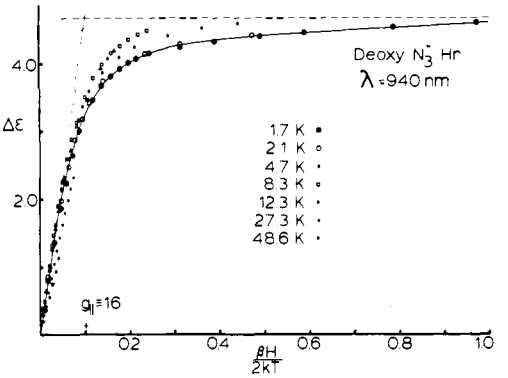

Figure 4. Saturation–magnetization curve for azidodeoxyhemerythrin. Intensity of MCD signal at 940 nm (see Figure 2 for conditions) plotted against $\beta H/(2kT)$. Data points shown were taken at 1.7 (●), 2.1 (○), 4.7 (■), 8.3 (□), 12.3 (△), 27.3 (·), and 48.6 K (▽) and at field values ranging from 6 to <0.1 T.

a rapid, dramatic change in the spectra occurs. This is shown in Figure 1b for addition of azide.

The deoxyN_3^- CD shows only a single symmetrical peak at 10 550 cm^{-1} ($\Delta\epsilon$ = 0.68 cm^{-1} M^{-1}). At liquid nitrogen temperature, the band is more intense and slightly higher in energy (ν_{max} = 10 800 cm^{-1}, $\Delta\epsilon$ = 0.96 cm^{-1} M^{-1}), but no additional features are resolved. The main absorbance feature has moved to lower energy with respect to deoxyHr, now appearing at about 10 600 cm^{-1} ($\epsilon \sim 22$ cm^{-1} M^{-1}) with a shoulder near 8500 cm^{-1} (ϵ = 6–7 cm^{-1} M^{-1}). The most significant finding is the disappearance of the feature near 5000 cm^{-1} in both the CD and absorbance. So in deoxyN_3^-Hr only two or three ligand field transitions are required by the combined CD and absorbance data.

The spectra in the presence of OCN^- are essentially identical with those for the N_3^- species. The CD shows a single band of identical energy, bandwidth, and intensity. By measuring CD changes at 940 nm during a titration with these anions, we find that N_3^- and OCN^- each bind with a single binding constant (K_B = 70 M^{-1}, pH 7.7 in each case), while F^- binds less strongly, with $K_B \sim 7$ M^{-1}. In addition the d–d spectrum of the F^- adduct[29] is definitely different than that in Figure 1b, as there is a transition present at higher energy in the CD ($\sim$11 600 cm^{-1}). It is difficult to assign exact transition energies, since even at 0.4 M F^- over 25% of the protein is still present as deoxyHr. Addition of N_3^- to the deoxyF^- protein shows that azide rapidly replaces F^-, giving the usual deoxyN_3^- spectrum.

MCD. The MCD for deoxyhemerythrin is shown in Figure 2. At 5 K the 5 T spectrum is coincident with the zero field data, which is simply the deoxy CD spectrum. However, at higher temperatures the 5-T trace is displaced from the CD base line, with the MCD signal being the difference between the two curves. The magnitude of this displacement increases with increasing temperature, reaching a maximum near 65 K, and then decreases at higher temperatures. The MCD intensity is plotted vs. temperature in Figure 3. The data are inherently noisy, due to the very small signal amplitude, but were reproducible over many samples from several different preps, and with either Cl^- or ClO_4^{2-} present as noncoordinating glassing agents.

The MCD spectra of the ligand bound forms of ferrous Hr are drastically different than that of deoxyHr. The deoxyN_3^- spectrum consists of two intense bands, which have identical temperature and magnetic field dependences (Figure 2). One has the same width and energy as the CD signal at 920 nm, and another peak is seen at 1031 nm, where no transition is seen in the CD. Both bands are roughly 40 times as intense as the deoxy signal and increase in intensity as the temperature is lowered. The signal saturates very easily, as shown in the form of a saturation–magnetization curve in Figure 4. In addition to ease of saturation, this figure shows that the data at various temperatures do not fall on the same curve and in fact form a set of nested curves. For constant values of H/T, the intensity increases slowly as the temperature is increased from 2 K, reaching a maximum at about 10 K, and then rapidly decreases at higher temperatures. In addition, there is a very intense MCD transition at 347 nm, which has the same field and temperature dependence as the ligand field bands, with 20 times the intensity. We were thus able to take high-quality data at a very low magnetic field (0.1 T or lower) and vary the temperature over a wide range, obtaining data essentially identical with that of the 920-nm band at 0.2 T shown in Figure 5. This allows us to separate effects induced by the field (e.g., mixing) from the Boltzmann population of low-lying excited states. Figure 5 does not show the "normal" Curie $1/T$ dependence as the temperature is increased, instead showing the intensity to drop at first abnormally slow and then too quickly at higher temperatures. The UV transition can also be seen in the absorption spectrum but is very weak with $\epsilon < 100$.

The MCD data for deoxyOCN$^-$Hr are shown in Figures 6 and 7. Again there are two d–d bands in the IR region, having the same energy and width as in deoxyN_3^-.[29] However, the magnetic field and temperature dependence is completely different (Figure 6). The 920-nm band shows no saturation with increasing field. In fact, with incremental increases in the magnetic field strength,

(29) See supplementary material.

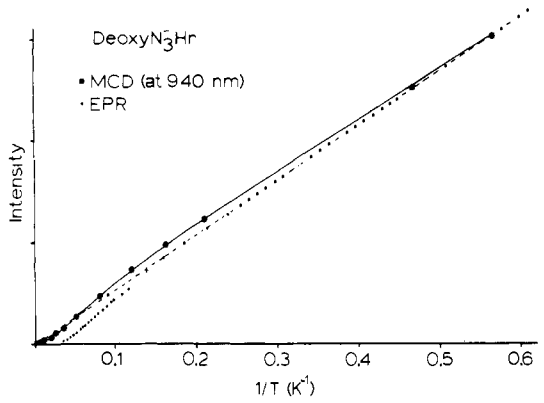

Figure 5. Temperature dependence of MCD (●) and EPR (·) intensities. The MCD points were measured at 940 nm (sample conditions detailed in Figure 2) at 0.2 T for a range of temperatures. The EPR points were measured at the point of maximum signal intensity (see Figure 8). The dashed line is the expected Curie law temperature dependence if only an isolated doublet ground state were populated.

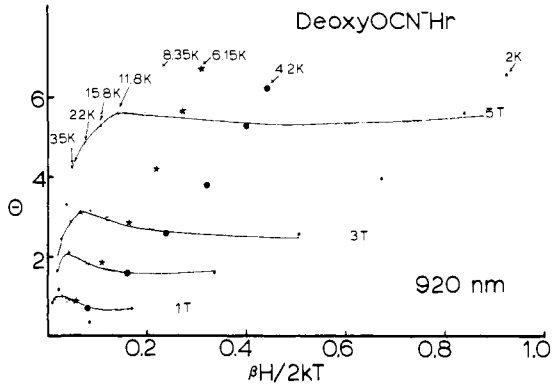

Figure 6. Saturation–magnetization curve for cyanatodeoxyhemerythrin MCD, measured at 920 nm.[29] Notice the curves are very nested and show "inverse saturation" as they curve upward with increasing field. The data was taken at 2 (•), 4.2 (●), 6.15 (*), 8.36 (□), 11.8 (+), 15.8 (▲), 22 (X), and 35 K (·) and at fields of 1, 2, 3, 4, 5, 5.5, and 5.66 T. The curves for 1, 2, 3, and 5 T are generated from the first set of ground-state parameters listed in the text.

the intensity increases by ever larger increments, resulting in "inverse saturation". For example, doubling the field from 2 to 4 T at 5 K more than doubles the signal size. Alternatively, if the field is held constant, the signal first increases as the temperature is lowered until a maximum is reached over 10 K. At still lower temperatures, the intensity first decreases slightly and then stays constant or increases slightly. The temperature of maximum intensity depends on the field. There is also a UV transition in deoxyOCN$^-$, at 320 nm, that shows the same field and temperature dependence as the 920-nm band but is about 20 times as intense.

The 1040-nm band shows even stranger behavior. At high temperatures it shows a similar intensity and similar inverse saturation behavior as the 920-nm band. At 4.2 K, there appears to be no signal from 0 to 3 T and a rapidly increasing signal at higher fields. The application of a small field at 1.8 K results in a negative signal, which gains intensity up to 3 T and then decreases so that by 6 T the signal is nearly back to the base line.

The MCD of the F$^-$ complex[29] shows a transition at approximately 850 nm which also shows an inverse saturation field dependence. Since this transition has a much lower intensity than the other ligand bound forms, the data are of lower quality and a thorough analysis is not attempted.

EPR. The deoxy, deoxyOCN$^-$, and deoxyF$^-$ complexes show no EPR absorbances at liquid nitrogen or liquid helium temperatures. However, the deoxyN$_3^-$ complex shows an intense, broad signal at very low field, with its maximum amplitude at 550 G (Figure 8). This signal has a shape that has been seen in a few high-spin Fe(II) complexes where $g_\perp = 0$.[30] The EPR

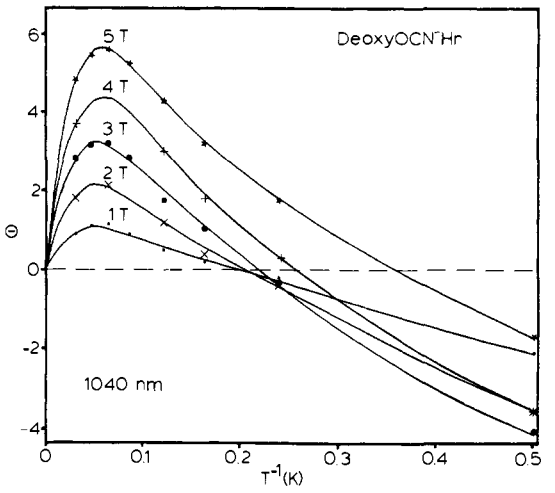

Figure 7. Temperature and magnetic field dependence of cyanatodeoxyhemerythrin MCD, measured at 1040 cm.[29] Notice that points of both positive and negative sign are included. The solid lines were generated from the parameters obtained from the least-mean-squares fit described in the text.

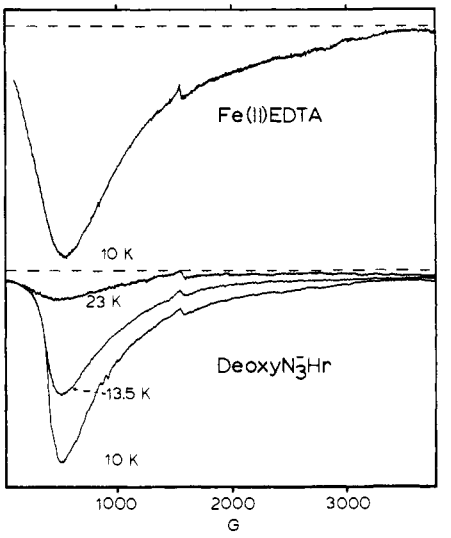

Figure 8. (top) EPR spectrum of 5 mM Fe^{II} EDTA at 10 K. Gain, 3.2 × 10^3; time constant, 20 ms; frequency, 9.388 gHz. (bottom) Variable-temperature EPR spectra for azidodeoxyhemerythrin. Above ~40 K the signal broadened and disappeared. Protein was 5 mM in 0.1 M Tris·SO$_4^{2-}$ pH 7.7 buffer, 0.2 M NaN$_3$. Gain, 2.5 × 10^3; other conditions the same. Both compounds were run as glycerol glasses.

for an Fe^{II}EDTA sample at the same concentration, power, and temperature is also shown in Figure 8, for comparison. Both signals are completely negative in sign and approach the base line assymptotically with increasing field. The Hr signal is most intense at lowest temperatures and loses intensity very rapidly as the temperature is increased, as shown in Figures 5 and 8. Finally, the signal broadens and disappears between 35 and 40 K. The signal is not easily saturated, showing no obvious power saturation even at 200 mW and 4.2 K.

Analysis

CD. Deoxyhemerythrin contains two ferrous irons, each of which is expected to contribute ligand field transitions in the IR spectral region. The resulting spectrum has three bands near 10000 cm^{-1} and a fourth near 5000 cm^{-1}. This spectrum is consistent only with the presence of one five-coordinate (bands at 10000 and 5000 cm^{-1}) and one six-coordinate (two bands near 10000 cm^{-1}) Fe(II). The 5000-cm^{-1} band seen in both absorbance

(30) (a) Hagen, W. R. *Biochim. Biophys. Acta* **1982**, *708*, 82–98. (b) Tinkham, M. *Proc. R. Soc. London, Ser. A* **1956**, *A235*, 535–548.

and CD immediately indicates that at least one iron in deoxyHr is either tetrahedral or five coordinate; however, tetrahedral geometry can be ruled out for several reasons. First, a tetrahedral iron should have no ligand field transitions to higher energy than the 5000-cm^{-1} band. This means the second iron in the active site would be responsible for all three transitions near 10 000 cm^{-1}, which cannot be achieved by a single Fe(II) of any coordination number. Second, the low intensity[15] of the 5000-cm^{-1} transition and the large isomer shift seen by Mössbauer studies[31] argue against four-coordinate geometries. Finally, the presence of three bands near 10 000 cm^{-1} requires that the second iron be six coordinate, as a five-coordinate Fe(II) should only exhibit one high-energy transition. The five- and six-coordinate active site picture is also consistent with Mössbauer[32] and intensity considerations.

The binding of anions to the Fe(II) site in deoxyHr causes complete disappearance of the 5000-cm^{-1} band in both CD and absorbance, while showing a single binding constant. This is not believed to be due to interactions with the protein backbone causing conformational changes, as other anions have no effect on the spectrum, even at high concentrations. This band has either moved to lower energy, by more than 1000 cm^{-1}, or there is no longer a low-energy transition upon anion binding. The combination of CD, absorbance, and MCD shows at least three (10 600, 8500, and 9600 cm^{-1}) and possibly four bands present near 10 000 cm^{-1}. These data are readily explained by both irons now being present in six-coordinate geometries, indicating that the five-coordinate iron in deoxyHr binds a single anion to become six coordinate. Alternately it is conceivable that another ligand is replaced by the incoming anion, and the resulting five-coordinate Fe(II) has its low-energy electronic transition at less than 4000 cm^{-1}. A band may be seen at this low energy in several five-coordinate model complexes. However, this requires either a very strong equatorial ligand field or a very weak total ligand field strength. It is unlikely that any non-heme protein would obtain the first characteristic, and since N_3^- and OCN^- are intermediate field ligands, the second possibility is also unlikely.

Spin Hamiltonian. In order to interpret the MCD and EPR results given above, we first consider the electronic structure of the ground state of a binuclear ferrous system: the energy levels and how they vary with magnitude of exchange interactions between irons, and mononuclear zero field splitting (ZFS) at each site. This was approached by use of the spin Hamiltonian[21]

$$\mathcal{H} = -2JS_1\cdot S_2 + D_1(S_{z1}^2 - \tfrac{1}{3}S(S+1)) + E_1(S_{x1}^2 - S_{y1}^2) + D_2(S_{z2}^2 - \tfrac{1}{3}S(S+1)) + E_2(S_{x2}^2 - S_{y2}^2) + g_1\beta H\cdot S_1 + g_2\beta H\cdot S_2 \quad (1)$$

where J is the exchange coupling constant, the subscripts 1 and 2 refer to the different irons, D and E are the axial and rhombic ZFS parameters, and H is the magnetic field strength. We assume that the exchange coupling is isotropic, but small anisotropic terms will simply combine with the ZFS parameters. This Hamiltonian was applied to an uncoupled basis set ($|M_{s1},M_{s2}\rangle$, M_s = 2, 1, 0, −1, −2), of the 5-fold spin degeneracy (assuming orbitally nondegenerate ground states) of each iron, and the resulting 25 × 25 matrix was diagonalized, producing energies and spin wave functions of the binuclear ground state.

As a first approximation, axial symmetry was assumed such that $E_1 = E_2 = 0$, and the D values for the two irons were set equal. The ZFS axes for the two irons are thus assumed parallel. The calculation was then performed over the complete range of D and J values for Fe(II). The results are shown graphically in Figures 9–11.[29]

Insight into these calculations can be obtained from the correlation diagram in Figure 9. The energy levels that result when exchange coupling is much larger than ZFS are shown at the left edge of the figure. Here the exchange is antiferromagnetic ($J < 0$) and the five multiplets that result have the total spin values

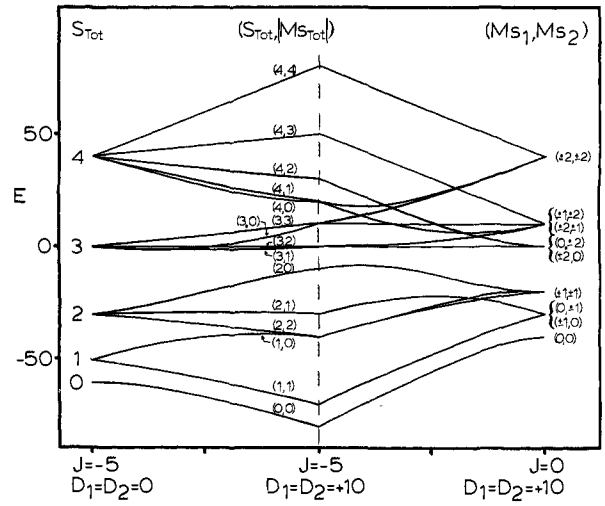

Figure 9. Correlation diagram of the binuclear ferrous ground state. The left side shows only the presence of exchange coupling ($-J$ = 5 cm^{-1}, $D_1 = D_2 = 0$ cm^{-1}), with multiplets labeled with their total spin values. The right side shows only field splitting ($D_1 = D_2$ = 10 cm^{-1}, J = 0), with states labeled with Ms values for each uncoupled iron (M_{s1}, M_{s2}). The central portion shows the splitting when both ZFS and exchange coupling are present ($-J$ = 5 cm^{-1}, $D_1 = D_2$ = 10 cm^{-1} at center) with states labeled as (S_{Tot},M_{sTot}) coupled wave functions.

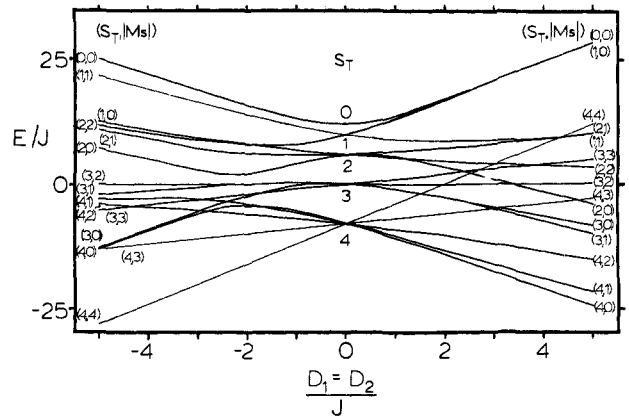

Figure 10. Energy levels of binuclear ferrous ground state and dependence on ZFS and exchange coupling parameters. The states are plotted in reduced variables, with the ordinate being energy (E/J) and the abscissa showing variation of ZFS (D/J). The exchange coupling (J) is held constant and the axial ZFS parameters on the two irons are constrained to be equal ($D_1 = D_2$) and range from $-5J$ to $5J$. Notice for ferromagnetic coupling the ground state is located at the bottom, while for antiferromagnetic coupling the ground state is at the top of the diagram. The spin Hamiltonian for calculating the levels is given in the text, with $E_1 = E_2 = 0$.

S_T = 0–4. These split into singlets and doublets as the axial ZFS is added, moving to the right on the diagram. These states are labeled by the dominant coupled spin wave functions (S_{Tot},M_{sTot}). The right side of the diagram shows the limiting case with large ZFS (D = +10 cm^{-1} on both irons) and no exchange coupling. These states are labeled by the uncoupled basis functions (M_{s1},M_{s2}) where 1 and 2 refer to the two irons. These levels are split as the irons begin to interact, with exchange coupling increasing to the left in the diagram. One can see the increasing complication of the splitting as the magnitudes of J and D become comparable. Diagrams such as Figure 10 are more useful for plotting the states for a wider range of parameters, including changing signs of D and J.

In Figure 10 we see the effect of varying the ZFS value for a constant J value. Both axes are in units of J, so that any ratio of D/J, from 0 to 5, can be found on the diagram. (For ratios larger than 5 where ZFS dominates, see the supplementary material.[29]) For axial ZFS with $D_1 = D_2$, all possible combinations of J and D can be located on the diagrams, and the energy

(31) Edwards, P. R.; Johnson, C. E.; Williams, R. J. P. *J. Chem. Phys.* **1967**, *47*, 2074–2082.
(32) Nicolina, C.; Reiff, W. M. *Inorg. Chem.* **1980**, *19*, 2676–2679.

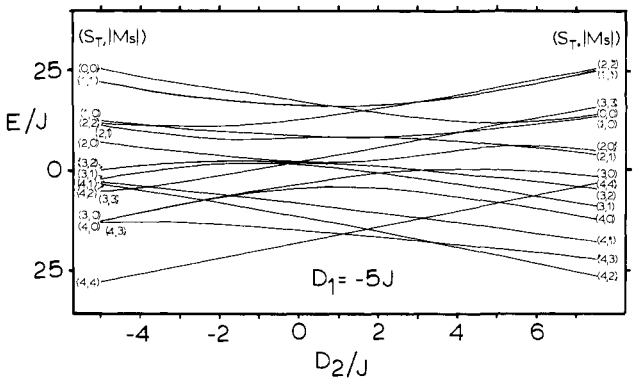

Figure 11. Energy levels of binuclear ferrous ground state and dependence on ZFS and exchange coupling parameters. All conditions are as in Figure 10, with exchange coupling held constant, but the axial ZFS parameter for one iron is fixed ($D_1/J = -5$), and the other D value is allowed to vary. Notice the left extreme of Figures 10 and 11 are identical as the parameters are the same.

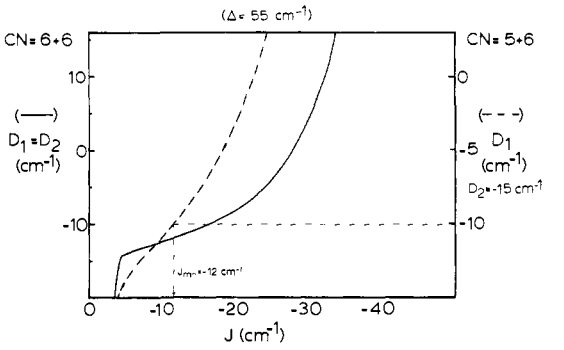

Figure 12. Curves showing the values of D and J which produce energy level splittings (see Figures 9–11) such that the first excited doublet is at 55 cm^{-1} from the singlet ground state. When the axial ZFS parameters for the two irons are constrained to be equal, the solid line results, with the appropriate parameters on the left ordinate. The dashed line is derived by setting $D_2 = -15$ cm^{-1} and allowing D_1 (left ordinate) to vary.

splittings and orderings can be obtained. As seen in the center of Figure 10, when $D = 0$ the exchange coupled ground state is evident, with the $S = 4$ manifold lowest in energy (when $J > 0$). When an axial distortion is applied, these states split, such that if $D < 0$ the $M_s = \pm 4$ doublet is the ground state as seen in the bottom left of the figure, with three more doublets and the $S = 4$, $M_s = 0$ ($|4,0\rangle$) singlet to higher energy. If $D > 0$, the $|4,0\rangle$ singlet is now the ground state. Therefore, for a binuclear complex with $J > 0$ and $D < 0$, we would expect a paramagnetic MCD signal at very low temperatures, while if D > 0, we would see no C-term signal at the lowest temperatures, if only the ground state was populated. The ground state is a singlet ($S_{Tot} = 0$) for any D value, when $J < 0$, as seen at the top of Figure 10. In this case ($J < 0$), since the D values are plotted as reduced parameters, the top right quadrant ground state correlates with negative ZFS ($D < 0$) and the top left with positive ZFS.

The next level of analysis is to allow the D values to vary for the two irons, still requiring axial geometry. In Figure 11, D_1 is set at $-5J$ and D_2 varies from $-5J$ to $7J$ along the abscissa. The left side of this diagram is identical with the left side of Figure 10, as the parameters are the same. While $D_2 < 0$ (and $J > 0$), the ground state is always $|4,\pm4\rangle$, but when D_2 becomes positive three different doublet ground states are possible ($|4,\pm4\rangle$, $|4,\pm3\rangle$, $|4,\pm2\rangle$), depending upon the relative magnitudes of the parameters, as shown at the lower right of the figure. Additional diagrams are required for different ratios of D_1 to J.

The last variable to be added is a rhombic distortion, which gives rise to the E_1 and E_2 values in eq 1. The remaining degeneracies are removed[29] when E is increased, as the $M_s = \pm n$ doublets are split. It is particularly interesting that while the ±1 and ±2 doublets split rapidly, the ±3 doublets split very slowly, and the ±4 doublet is barely split, even with "maximum rhombicity" of $E/D = {}^1/_3$. This is because the S_x^2–S_y^2 term in the Hamiltonian mixes states with $\Delta M_s = \pm2$, and so the $M_s = \pm4$ doublet levels mix only with $M_s = \pm2$ doublets in first-order and with each other in higher order terms. This means the ±4 and perhaps ±3 states may be treated as pseudodoublets even in fairly low symmetry and that the rhombic term has little effect on the energy splittings between "doublets", the pairs splitting out approximately around their mean energy.

A final complication arises if we remove the assumption that the ZFS axes for the irons in the site are parallel. This is addressed by eliminating the constraint that $E_2 \leq 3D_2$. This effectively allows the iron-2 ion to take any orientation relative to the constrained iron-1 ion. Calculations of this situation show only small changes from the diagrams given above.

These diagrams, and analogous ones not shown,[29] may now be used to study the MCD and EPR data for the various species studied to interpret the field and temperature dependence observed.

MCD. Deoxyhemerythrin. The data presented in Figure 2 show that, at high fields and very low temperatures, deoxyHr has no MCD signal. However, as the temperature is increased a small signal is evident. This indicates that the ground state is a singlet energy level and is supported by EPR, Mössbauer, and magnetic susceptibility results, which indicate a diamagnetic state at very low temperatures. However, the MCD signal shows that a paramagnetic "doublet" is populated at higher temperatures. The data were taken with constant magnetic field, while the temperature was varied from 4.2 to 150 K. This essentially reduces the problem to a case of thermally populating a constant set of energy levels and extracting the splitting of the levels. The high noise level in the data precludes an exact fitting of the signal temperature dependence. However, in several independent experiments, the signal reaches maximum intensity at 65 K and then decreases with a roughly $1/T$ dependence, indicating the first excited doublet is at about 55–65 cm^{-1} above the ground state.

For a Fe(II) dimer, it is possible to produce a singlet ground state and paramagnetic excited state with either ZFS of each mononuclear iron or antiferromagnetic exchange between irons. If the irons are uncoupled and ZFS is solely responsible for the splitting, D = 40–60 cm^{-1}, which is physically unreasonable for ferrous iron, as indicated earlier. If the splitting is due only to exchange coupling, we find $-J$ = 20–30 cm^{-1}. However, we know that both ZFS and exchange coupling can be significant in this case. Therefore, in order to extract the ground-state parameters from this result, all values of D and J resulting in a doublet excited state 55–65 cm^{-1} above a singlet ground state were located. The results are given in Figure 12, where the solid curve represents the values of J and D required to reproduce the experimental splitting of 55 cm^{-1}. J must be less than 0, the reason for this being clear from Figure 10. When $J > 0$ and $D < 0$, only doublet ground states are possible (lower left), but when $D > 0$, a $|4,0\rangle$ singlet state results as shown at the bottom right of the diagram. However, the energy splitting to the $|4,\pm1\rangle$ doublet is almost totally dependent on D, and to get a 40–60-cm^{-1} splitting requires $D_1 = D_2$ = 60–90 cm^{-1}, again an unreasonable value.

When $J < 0$ and $D > 0$, the ground state is $|0,0\rangle$ and the first excited state is the $|1,\pm1\rangle$ doublet (upper left, Figure 10). Since these originate from different exchange split multiplets ($S_T = 0,1$), the splitting is mostly due to J, with less dependence on D, as shown in the diagrams. Thus, in Figure 12 we see for positive D, J is large and negative and fairly insensitive to changes in D. This region with large positive D values sets an upper limit for the exchange coupling at $-J \sim 38$ cm^{-1} (for a 65-cm^{-1} $|0,0\rangle \rightarrow |1,\pm1\rangle$ splitting).

Finally, it is possible that both D and J are negative (upper right, Figure 10). This gives rise to the lowest values of J and thus is of importance for assigning a lower limit of the exchange coupling constant. Figure 10 shows that the splitting can be relatively large for small values of D and J in this regime. In this case the $|0,0\rangle$ and $|1,0\rangle$ singlets are very close in energy but neither contributes to the MCD signal. The lowest excited doublet is either $|2,\pm1\rangle$ or $|4,\pm4\rangle$, depending on relative values of J and D. Since the

diamagnetic ground state is now accidentally doubly degenerate (the above-mentioned singlets), the Boltzmann distribution is changed such that the lowest excited state must be near 56 cm^{-1} in order to fit the MCD data. We see from Figure 12 that, with very large negative D values, the magnitude of $-J$ may be as small as 3 or 4 cm^{-1}, but these D values are again unreasonably large. The dashed curve in Figure 12 is generated by fixing one D value at -15 cm^{-1}, the largest axial ZFS observed for six-coordinate Fe(II), and varying the remaining ground-state parameters to give rise to an excited-state doublet at 55 cm^{-1}. The plot is a function of the exchange coupling and D_1: the axial ZFS of the five-coordinate Fe(II). Selecting the largest observed value for five-coordinate ferrous complexes of -10 cm^{-1} sets a lower limit for $-J$, which must be at least 12 cm^{-1} to fit the MCD temperature dependence. This means we can define a range of possible values for J in deoxyhemerythrin, as $-J \sim 12$–38 cm^{-1}. The limits for more typical D values[33] of 7 cm^{-1} (vide infra) are $-J = 18$–33 cm^{-1}.

Azidodeoxyhemerythrin. The analysis of the deoxyN_3^-Hr MCD results begins by observing the doublet character of the ground state. The 1.7 and 2.2 K data have nearly the same temperature and field dependence as shown in Figure 4. This indicates that the excited spin states have little or no population near 2 K. The saturation–magnetization curve can then be used to obtain a rough estimation of the ground-state g value, as previously shown by Thomson.[23] By applying this treatment and assuming completely anisotropic g values, as is reasonable for a low-symmetry non-Kramers system and consistent with the line shape of the EPR spectrum of deoxyN_3^- (Figure 8), we find $g_{\parallel} > 15$. This treatment is only rigorously correct for an allowed xy-polarized transition from an isolated Kramers doublet, assumptions which certainly are not correct for a coupled Fe(II) system. However, these deviations from the idealized parameters should not significantly increase the apparent effective g value obtained.[23a] This g value is clearly too large for an $S = 2$ Fe(II) ion and, therefore, requires exchange coupling, giving a total spin $S = 4$ system, which is also consistent with the EPR results (vide supra). All of the data indicate an $M_s = \pm 4$ doublet ground state and therefore ferromagnetic exchange coupling, with the temperature dependence indicating that at least two other states can be thermally populated.

It is possible to estimate values for the ZFS and exchange coupling constants by fitting the MCD temperature and field dependence[23c] (Figure 5). A check of the J vs. D diagrams (Figures 10 and 11, bottom left) shows that whenever the $|4,\pm4\rangle$ doublet is lowest, the $|4,\pm3\rangle$ state is the first excited doublet level. The data were thus fit to the three doublets $|4,\pm4\rangle$, $|4,\pm3\rangle$, and $|4,\pm2\rangle$, where the zero field energies of the doublets (E_{M_s}, where E_4 is set to zero) were allowed to vary, as were the MCD intensities (A_{M_s}) arising from each of the three doublets. This is shown in eq 2 where $^2/_3$ in the exponent approximates the effects of orientation averaging in the MCD intensity. These five parameters were varied to obtain the best least-mean-squares fit to the data points. It was found that the 0.1-T data at 347 nm and the 0.2-T data at 920 nm (the lowest field used in each case) fit nicely to a ground $|4,\pm4\rangle$ level, a $M_s = \pm3$ doublet at 8.3 cm^{-1} giving an MCD signal about 3 times as intense as the ground state, and the $M_s = \pm2$ doublet at 16 cm^{-1} having a larger MCD signal, of the opposite sign. The data cannot be fit adequately with less than three doublets, which further supports the irons being coupled. The fit is very sensitive to the energy and intensity of the ground and first excited levels and less sensitive to that of the $M_s = \pm2$ doublet. The values found for the $|4,\pm2\rangle$ levels by fitting the data

$$I = \Big(\sum_{M_s=2,3,4} A_{M_s}\{\exp[-(E_{M_s} - {}^2/_3|M_s|g\beta H)/kT] - \exp[-(E_{M_s} + {}^2/_3|M_s|g\beta H)/kT]\}\Big)/\Big(\sum_{M_s=2,3,4} \exp[-(E_{M_s} - {}^2/_3|M_s|g\beta H)/kT] + \exp[-(E_{M_s} + {}^2/_3|M_s|g\beta H)/kT]\Big) \quad (2)$$

Table I.

	J, cm^{-1}	D_1, cm^{-1}	D_2, cm^{-1}
deoxyHr	-12 to -38	*a*	*a*
deoxyN_3^-Hr	>1	-3^b	-3^b
		-7^b	$+7^b$
deoxyOCN$^-$Hr	>1	$+5^b$	$+5^b$
		-13	$+10$
deoxyF$^-$Hr	>1	$<0^c$	$>0^c$

[a] Cannot be estimated due to large magnitude of exchange coupling. [b] The value for one iron may increase slightly if the other decreases. [c] Data do not allow good estimate.

are best thought of as weighted average values for a number of closely spaced levels, as seen in Figure 10 (bottom left).

These energy splittings, in combination with the J vs. D diagrams, show that for deoxyN_3^-hemerythrin $D_1 = D_2 = -3$ cm^{-1}, if the parameters are equal. If D_1 increases, D_2 must decrease, up to limiting values of $D_1 = -7$ cm^{-1} and $D_2 = -2$ cm^{-1}. In addition, in order to produce the proper energy orderings,[34] $3J > D$ is required. Therefore, $J > 1$ cm^{-1}, although no upper limit can be determined.

Cyanatodeoxyhemerythrin. The deoxyOCN$^-$ data are much more complicated, and the fitting of the unusual temperature and field dependence was done by systematically investigating all possibilities for a two iron system, both coupled and uncoupled. The complicated constant field temperature dependence shown in Figures 6 and 7 requires population of several very closely spaced energy levels. This temperature dependence cannot be fit with a single Fe(II), which has only a singlet and two doublet energy levels. Thus, both irons must contribute at each of the very different looking transitions. Further, it was not possible to simultaneously fit the data at all wavelengths assuming two uncoupled irons. The results at each wavelength could be fit adequately with two irons, but the parameters which gave a good fit at one wavelength gave a clearly unsatisfactory fit at the other. The 1040-nm peak would be adequately fit with $D_1 = 2$ cm^{-1} and $D_2 = 6$ cm^{-1}, while the 920-cm transition required $D_1 = 2$ cm^{-1} and $D_2 = 16$ cm^{-1}. Thus, the data require an exchange coupled pair of irons, in which case the same set of states must generate the very different looking MCD spectra at 920 and 1040 nm.

The variable-temperature data at high field in Figure 6 show that there are still very low-lying excited states. This eliminates situations in which the ground state has greater M_s than the excited states, in which case the ground state would become isolated by 6 T. The J vs. D diagrams indicate several regions where the coupled Fe(II) system has closely spaced energy levels with low-lying excited states having greater spin than the ground state. This causes a crossing over of levels as the field is increased, resulting in closely spaced levels at all fields. The data were then least-squares fit much as for deoxyN_3^-, requiring the same energy levels to fit both bands, for all magnetic fields. It was found that the data could be adequately fit in three different ways. The best fit was obtained with a $M_s = \pm2$ ground doublet, a $M_s = \pm3$ excited state at 3–4 cm^{-1}, and a $M_s = \pm4$ doublet at ~ 16 cm^{-1}. This corresponds to $J = 1$–2 cm^{-1}, $D_1 \sim 7$ cm^{-1}, and $D_2 \sim -7$ cm^{-1} (Figure 11, lower right). The solid lines in Figures 6 and 7 are the fit obtained by using these parameters in eq 2, showing all the features in these plots can be reproduced. Again the highest doublet should be thought of as a weighted average of states but was required for a reasonable fit. Another situation which produced nearly as good of fit consists of a singlet ground state and $M_s = \pm1$, ±2, and ±3 excited states at 2, 7, and 25 cm^{-1}, respectively, which corresponds to $J > 2$ cm^{-1}, $D_1 = 4$–6 cm^{-1}, and $D_2 = 6$–3 cm^{-1}. Again here at least three doublets are required for an acceptable fit. The third adequate fit, less satisfactory than the above two, is included in Table I. All adequate fits for deoxyOCN$^-$Hr then gave ferromagnetic exchange coupling con-

(33) For high-spin Fe(II), since the splitting arises from coupling with the excited ligand field states,[19a] which are at higher energy in lower symmetry, axial ZFS typically decreases as the complex symmetry decreases. Since the protein site is certainly of low symmetry, we expect fairly small ZFS.

(34) The top left of Figure C[29] shows that only when $3J > D$ is the first excited state the $|4,\pm3\rangle$ doublet, previously being two singlet states which give rise to no MCD signal. The T dependence of the MCD clearly indicates the first excited state is a state producing an MCD C term.

stants ($J > 0$) and show at least one D value must be positive.

One should note that the crossing of ground-state M_s levels will reproduce all the unusual magnetic field dependence observed in Figures 6 and 7: the inverse saturation and the negative and then positive signal seen at 1040 nm. In addition, field-induced mixing will certainly contribute to both of these effects considering the close spacings of energy levels. Such "B-term" behavior has not been included in the fit to the data and would change the parameters obtained: thus, the D values should be considered as approximations. However, even with field-induced mixing, the data still require crossing of levels, and no other combination of parameters will satisfactorily produce this. Therefore, all adequate fits for deoxyOCN$^-$Hr require ferromagnetic exchange coupling constants ($J > 0$) and at least one positive D value.

The data for deoxyF$^-$ were not of sufficient quality to extract reliable constants. However, the temperature dependence of the signal indicates a paramagnetic ground state and thus lack of strong antiferromagnetic coupling. In addition, the lack of saturation behavior and absence of EPR signals indicates the ground state is not $|4,\pm4\rangle$ and is likely $M_s = \pm2$. This can be fit with $J > 0$, $D_1 > 0$, and $D_2 < 0$, much as in deoxyOCN$^-$Hr. The spin-Hamiltonian parameters estimated from the temperature-dependent MCD spectra are collected in Table I.

EPR. The deoxyN$_3^-$Hr MCD field- and temperature-dependent data require a $|4,\pm4\rangle$ doublet ground state. The temperature dependence of the EPR signal (Figure 5) shows that the intensity must arise from the ground state and thus is a highly forbidden $\Delta M_s = \pm8$ transition. Since only a $\Delta M_s = \pm1$ transition is allowed in the normal configuration of the EPR experiment, there must be components of this transition mixed into the $|4,\pm4\rangle$ ground state, by low-symmetry ligand field and perpendicular components of the magnetic field. It is useful to compare the intensity mechanism of this transition with that of the "$\Delta M_s = \pm4$ transition" seen in a few mononuclear Fe(II) complexes.[30]

The transition within the $M_s = \pm2$ level in mononuclear ferrous iron complexes is allowed because of rhombic symmetry,[17] in which the $(S_x^2 - S_y^2)$ term of the Hamiltonian mixes the $|2,0\rangle$ level into the $|2,\pm2\rangle$ doublet, and the H term in $\mathcal{H}_{zeeman}$, which mixes states with $\Delta M_s = \pm1$. The mixing due to rhombic distortion, and thus the transition intensity, is proportional to E/D, while the splitting of the pseudodoublet is proportional to E^2/D. Therefore, as the rhombic distortion in an $S = 2$ complex increases, the EPR intensity will increase until the $M_s = \pm2$ states splitting ($\Delta = 3E^2/D$) is larger than the microwave frequency, at which point the transition can no longer be observed. For the $S = 4$ system, the "$\Delta M_s = \pm8$ transition" should be inherently much less intense for a given E value, because the rhombic ZFS term can mix the $|4,0\rangle$ state with the $|4,\pm4\rangle$ doublet only in fourth order. Fourth-order perturbation theory on the $S_T = 4$ manifold predicts the rhombic splitting given by relation 3, where E is now the

$$\Delta \propto E^4/[(W_{4-2})^2(W_{4-3})] \quad (3)$$

rhombic ZFS parameter of the dimer and W_{i-j} is the energy difference between the $M_s = \pm i$ and $\pm j$ ground levels. This, however, neglects the dependence on exchange coupling, which is significant for small J values. Calculating the splitting analytically with parameters reasonable for deoxyN$_3^-$Hr gives eq 4

$$\Delta = FE^4/D^2 \quad (4)$$

(when $J \leq 3D$) where F is a function of the exchange coupling ($F = 0.57$ cm for $J = 1$ cm^{-1} and decreases slowly as J increases), and E and D are the mononuclear ZFS parameters. It is clear that for a given set of parameters the rhombic splitting is roughly an order of magnitude smaller for the $S = 4$ than for the $S = 2$ system. Thus, $S = 4$ complexes with large E values and thus relatively large intensity can have Δ values of <0.3 cm^{-1} such that, in contrast to the monomer, an X-band transition can occur.

A comparison of the EPR intensity arising from a $S = 4$ coupled system having representative parameters with that from a $S = 2$ system, where signals have been seen for some complexes,[30] can be obtained by diagonalizing the spin Hamiltonian for $S = 2$ and 4 systems. Parameters are chosen[35] to give a rhombic splitting (Δ) of 0.2 cm^{-1} in the ground state ($|2,\pm2\rangle$, and $|4,\pm4\rangle$ respectively) of each system, so that an X-band transition can still occur. In order to obtain the same rhombic splitting (Δ), the rhombic term (E) is larger in the binuclear system than in the $S = 2$ system (1.8 as compared to 0.64 cm^{-1}). The wave functions for the two components of the mononuclear ground state are $\Phi^+ = \sum C_{M_s}|M_s\rangle$ and $\Phi^- = \sum C'_{M_s}|M_s\rangle$, and eq 5 then gives the calculated intensity

$$I = \Gamma|\langle\Phi^+|(S_+ + S_-)|\Phi^-\rangle|^2 = \Gamma[\sum(\alpha(C_iC'_j)\delta_{(i,j\pm1)})]^2 = \Gamma K_{\pm4} \quad (5)$$

of the EPR signal. Here α is the coefficient generated by raising and lowering operators, Γ contains the concentration and temperature dependence of the intensity, as well as other fundamental constants, and $K_{\pm4}$ is obtained from the evaluation of the transition moment integral over the appropriate wave functions. In the $S = 4$ systems, only those coefficients of the uncoupled basis in the $M_s = \pm4$ ground state wave functions $\phi^+ = \sum C_{M_{s1},M_{s2}}|M_{s1},M_{s2}\rangle$ and $\phi^- = \sum C'_{M_{s1},M_{s2}}|M_{s1},M_{s2}\rangle$ which give rise to $\Delta M_s = \pm1$ single center transitions with no spin change on the second iron contribute to the transition intensity. This is shown in eq 6, where β is

$$I = \Gamma|\langle\phi^+|(S_+ + S_-)|\phi^-\rangle|^2 = \Gamma\{\sum[\beta(C_{ij}C'_{kl})\delta_{ik}\delta_{(j,l\pm1)} + \beta'(C_{ij}C'_{kl})\delta_{(i,k\pm1)}\delta_{jl}]\}^2 = \Gamma K_{\pm8} \quad (6)$$

generated by the raising and lowering operators, and Γ and $K_{\pm8}$ are as in eq 5. Therefore, the intensities of the $\Delta M_s = \pm8$ and ±4 transitions are proportional to $K_{\pm8}$ and $K_{\pm4}$. For the calculations outlined above, the $S = 4$ system has an $\sim$50% greater $K_{\pm8}$ coefficient than the $K_{\pm4}$ coefficient for the monomer. Figure 8 shows the EPR spectra for the monomer Fe^{II}EDTA complex and the dimeric deoxyN$_3^-$Hr, and the intensity is indeed similar. When J is increased in the above calculation, the intensity is found to decrease slightly, as does the probability in the mononuclear case if D is increased. We find that an EPR spectrum should in principle be observable in ferromagnetically coupled binuclear ferrous systems, assuming relaxation properties are favorable, when axial ZFS for both irons is negative. For the deoxyOCN$^-$ and deoxyF$^-$ derivatives, at least one D value is positive, resulting in a $M_s = \pm2$ or 0 ground level, neither of which should give rise to EPR intensity.

Discussion

The CD and absorption data detailed above show that the deoxyhemerythrin active site has one five-coordinate and one six-coordinate ferrous iron. The magnetic data show that the native ferrous protein has a diamagnetic ground state, due to the irons being antiferromagnetically coupled with $-J = 12$–38 cm^{-1}. We showed before[12] that exchange coupling of this magnitude was indicative of a hydroxo bridge. A close look at the active site shows that the only likely bridging groups capable of being present at the site are the carboxylates and water-based ligands (O^{2-}, OH^-, and H_2O), since a major structural reorganization is needed for other protein ligands to reach the site, and the electron density difference map of the deoxy site shows that this has not occurred.[10] In Fe(II) compounds containing bridging carboxylates,[36] usually in linear chain systems, the exchange is always weak and often ferromagnetic. The two bridging carboxylates in hemerythrin should be able to contribute at most only a few wavenumbers to the coupling constant. Model complexes show, however, that hydroxo bridges are capable of mediating exchange of the required magnitude of -15 to -35 cm^{-1}. We expect the coupling for a μ-OH$^-$Fe^{II} dimer to be up to 50% larger than in the Fe(III) dimers, where the J values are found[37] to vary from -10 to -18 cm^{-1}. This

(35) The magnetic field was set at 1 rad from the Z axis, at 2000 G for the $S = 2$ case and 1000 G for the $S = 4$ model, so that the splitting was equal in each case. For the $S = 2$ system D was set at -6 cm^{-1}, an average small value, requiring $E = 0.64$ cm^{-1} ($E/D = 0.106$) to give $\Delta = 0.2$ cm^{-1}. For the $S = 4$ system, parameters reasonable for the deoxyN$_3^-$ derivative were chosen, with $J = 1$ cm^{-1}, $D_1 = D_2 = -5.3$ cm^{-1}, and $E/D = 1/3$.

(36) (a) Cheng, C.; Reiff, W. M. *Inorg. Chem.* **1977**, *16*, 2097–2103. (b) Pierce, R. D.; Freidberg, S. A. *Phys. Rev. B: Solid State* **1971**, *3*, 934–942. (c) Barros, S. d. S.; Freidberg, S. A. *Phys. Rev.* (1966) *141*, 637–640.

can be seen from the relation of the many electron J to the one-electron J_{ij}, where these can be treated as the interactions between the singly occupied orbitals on the two irons, through the bridging ligands.[38] Here n is the number of unpaired electrons

$$J = (1/n^2)\sum_{ij} J_{ij} \quad (7)$$

at each site and i and j are the electrons on each center. Since the above relation will be dominated by a few J_{ij}, to a rough approximation the exchange coupling will be inversely proportional to the square of the number of unpaired electrons at the metal ions.

Although an oxo bridge cannot be ruled out, a hydroxo bridge seems much more likely for several reasons. First the reduction of both irons should raise the pK_a of the bridge by at least several log units, making protonation more likely.[39] Further, the exchange coupling for the oxo-bridged ferric dimers ($-J \sim 100$ cm^{-1})[40] is an order of magnitude larger than the corresponding hydroxo-bridged dimers. For the same reason as mentioned above, coupling for a oxo-bridged ferrous dimer should be even larger and probably too large for the data on deoxyHr ($-J < 38$ cm^{-1}). Alternatively, further protonation to an aquo bridge should generate only very weak coupling.

The EXAFS data[41] are consistent with the above picture. The disappearance of the short 1.8-Å Fe–O bond length and the intervening atom effect is reported. There is, however, an increase in the number of 2.0-Å Fe–O distances, which is consistent with replacement of the O^{2-} with the hydroxo bridge. The data also indicate the five histidine ligands remain similarly bound upon reduction. On the basis of the CD and absorbance which shows five- and six-coordinate irons and the EXAFS data, the deoxy structure is likely similar to the metaquo site, with the oxo bridge protonated and the irons reduced and all other ligands essentially unchanged. In addition the recent low-resolution X-ray difference map shows only minor differences between the deoxy and metaquo sites.[10]

This is also supported by the work of Wieghardt and co-workers, who have succeeded in synthesizing a bis(μ-carboxylato)-μ-hydroxo ferrous dimer,[42] which has spectral features very similar to those present in deoxyhemerythrin, and shows fairly large antiferromagnetic exchange. However, it is difficult to compare these values, as the ZFS of the Fe(II) still has to be taken into account.

We have shown that N_3^-, OCN^-, and F^- bind to deoxyhemerythrin with a single binding constant, likely binding to the open coordination position on the five-coordinate iron in deoxyHr, resulting in hexacoordination. In addition a large change is seen in the magnetic properties of the protein, indicating a new ground state. The cyanate complex shows behavior consistent with a $|4,\pm2\rangle$ ground state, while the azide complex has a $|4,\pm4\rangle$ ground state. Both of these ground states require ferromagnetic exchange coupling, while the difference in properties in going from N_3^- to OCN^- arises from the change in sign of the ZFS D value of at least one iron.

In very low-symmetry complexes, such as proteins, some excited-state orbital doublet character mixes into the orbital singlet ground state, decreasing the magnitude of the axial ZFS parameter. Rudowicz has calculated[43] the spin-Hamiltonian parameters for a complex with trigonal plus low-symmetry distortions, including substantial amounts of orbital mixing. With pure trigonal character,[19] D is large and positive ($\sim$10–14 cm^{-1}), but with sufficient low-symmetry mixing, the D value decreases and can actually become negative (~ -7 cm^{-1}).[43] The low-symmetry protein complexes would be expected to have small D values, as is seen here, and the change in sign of D upon exchanging N_3^- and OCN^- might result from a difference in binding geometry. Azide is known[44] to bind to transition metals in a bent manner, while cyanate[45] typically binds linearly. Therefore, even though the ligand field strengths of N_3^- and OCN^- are similar, resulting in apparently identical transition energies and widths, the actual low-symmetry distortion of the complexes can be different, resulting in different ZFS magnetic ground-state properties.

Chart I

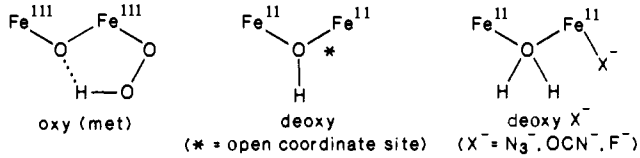

The disappearance of the large antiferromagnetic exchange coupling and resulting small ferromagnetic exchange, upon binding of F^-, N_3^-, or OCN^-, is indicative of a large perturbation in the dominant superexchange pathway: the hydroxo bridge. One possible explanation is that the bridge angle decreases significantly, nearing 90°. There should be some angular dependence in the size of exchange mediated by a bridge between Fe(II)s.[38b,46] In particular the antiferromagnetic component of the exchange would be expected to decrease with decreasing bond angle. In a series of cupric complexes,[47] the coupling becomes ferromagnetic at angles less than $\sim$96°. However, this would require the iron–iron distance to decrease from $\sim$3.25 to about 2.95 Å upon binding anions. EXAFS would be useful in probing this possibility. An alternative possibility, which we favor, is that binding of anions raises the pK_a of the bridging ligand, as is known to occur in transition-metal complexes.[39] This could lead to protonation of the hydroxo bridge, giving a bridging H_2O between irons, or breaking the bridge entirely. Although it would explain the magnetic data, it seems less likely that the bridge is broken, since CD shows the ligand bound forms likely contain two six-coordinate irons. This means that if the bridge breaks, an additional ligand (OH^- or H_2O) must bind to the iron, which would be difficult in this crowded site. An aquo bridge would result in two six-coordinate irons, with significantly reduced exchange coupling. Water is known to bridge ferrous irons in at least one linear chain compound[48] and result in very weak ferromagnetic exchange. The μ-aquo-bis(μ-carboxylato) structure is observed as a stable structure for a number of Co(II)[49] and Ni(II)[50] dimers with a ligand set similar to Hr, as well as a number of other metals.[51] Since the pK_a's of water bound to Co(II) and Ni(II) bracket that of Fe(II),[39] it is reasonable that the bridge in ferrous hemerythrin is diprotonated.[52] This rationale leads us to Chart I for Hr

(37) (a) Armstrong, W. H.; Lippard, S. J. *J. Am. Chem. Soc.* **1984**, *106*, 4632–4633. (b) Schugar, H. J.; Rossman, G. R.; Gray, H. B. *J. Am. Chem. Soc.* **1969**, *91*, 4564–4566. (c) Chiari, B.; Piovesana, O.; Tarantelli, T.; Zanazzi, P. F. *Inorg. Chem.* **1983**, *22*, 2781–2784.

(38) (a) Anderson, P. W. *Solid State Phys.* **1963**, *14*, 99. (b) Hay, P. J.; Thibeault, J. C.; Hoffman, R. *J. Am. Chem. Soc.* **1975**, *97*, 4884–4899. (c) Kahn, O.; Briat, B. *J. Chem. Soc., Faraday Trans. 2* **1976**, *72*, 1441–1446. (d) Gleizes, A.; Verdaguer, M. *J. Am. Chem. Soc.* **1984**, *106*, 3727–3737.

(39) Basolo, F.; Pearson, R. B. Mechanisms of Inorganic Reactions; Wiley: New York, 1967; pp 32–33.

(40) (a) Murray, K. S. *Coord. Chem. Rev.* **1973**, *12*, 1–37. (b) Schugar, H. J.; Rossman, G. R.; Barraclough, C. G.; Gray, H. B. *J. Am. Chem. Soc.* **1972**, *94*, 2683–2690.

(41) (a) Elam, W. T.; Stern, E. A.; McCallum, J. D.; Sanders-Loehr, J. *J. Am. Chem. Soc.* **1982**, *104*, 6369–6373. (b) Co, M. S. Ph.D. Thesis, Stanford University, 1983.

(42) Chaudhari, V. P.; Wieghardt, K.; Nuber, B.; Weiss, J. *Angew. Chem.* **1985**, *97*, 774–775.

(43) Rudowicz, C. *Phys. Rev. B* **1980**, *21*, 4967–4975.

(44) Dori, Z.; Ziolo, R. F. *Chem. Rev.* **1973**, *73*, 247–254.

(45) Anderson, S. J.; Brown, D. S.; Finney, K. J. *J. Chem. Soc., Dalton Trans.* **1979**, 152–154.

(46) Hodgson, D. J. *Magneto-structural Correlations in Exchange Coupled Systems*; Willet, R. D., Gatlesche, D., Kahn, O., Eds.; Reidel: New York, 1983; pp 497–522.

(47) Hatfield, D. J. in *Extended Interactions between Metal Ions in Transition Metal Complexes*; Interrante, L. V., Ed.; American Chemical Society: Washington, DC, 1974; pp 108–141.

(48) Morelock, M. M.; Good, M. L.; Trefonas, L. M.; Magesle, R.; Karraker, D. G. *Inorg. Chem.* **1982**, *21*, 3044–3050.

(49) (a) Turpeinen, U.; Ahlgren, M.; Hamalainen, R. *Acta Crystallogr., Sect. B* **1982**, *B38*, 1580–1583. (b) Ahlgren, M.; Hamalainen, R.; Turpeinen, U. *Finn. Chem. Lett.* **1983**, 125–128.

(50) Turpeinen, U.; Ahlgren, M.; Hamalainen, R. *Finn. Chem. Lett.* **1977**, 246–251.

(51) Albers, M. O.; Liles, D. C.; Singleton, E.; Yates, J. E. *J. Organomet. Chem.* **1984**, *272*, C62–C66.

derivatives. This chart reflects the effects that changing the electron density at the irons will have on the pK_a of the bridging oxygen atom. Water bound to the highly charged ferric ion tends to be fairly acidic, with the hexaquoferric anion having a pK_a of 2.2, whereas the pK_a of the hexaquoferrous ion is 9.5. The presence of two ferric ions bound to a single oxygen atom is known to leave it completely depronated in the met form. However, reducing the protein to deoxyhemerythrin, resulting in two ferrous ions, raises the pK_a of the oxo bridge and leads to its protonation. Binding anions can also increase the electron density on the metal. Studies have shown that binding anions, or simply changing the binding geometry, can raise the pK_a of other bound ligands by 2–3 log units.[39] Therefore, the binding of N_3^- or OCN^- to the five-coordinate Fe(II) in deoxyhemerythrin would raise the pK_a of the bridging oxygen, which could result in additional protonation of the hydroxide.[53]

Chart I is also consistent with previous reports[54] which indicate that the bridge does not exchange with solvent water in the met oxidation state and exchanges very slowly in deoxyHr but exchanges rapidly in the presence of N_3^- and OCN^-. OH^- bound to transition-metal ions is known to exchange relatively slowly,[55a] while H_2O exchanges about 3 orders of magnitude faster.[55] Although OH^- on mononuclear Fe(II) does exchange fairly rapidly, when it is bridging to two atoms, in the deoxyHr active site pocket, the exchange rate appears to be significantly reduced.

There do appear to be two points of difficulty in relation to the earlier kinetic data. CD and MCD show that F^- binds to deoxyhemerythrin but apparently does not cause rapid exchange of the bridge. This, however, is consistent with the observation that F^- binds differently than OCN^- or N_3^-, as indicated by its reduced binding constant and much lower energy ligand field transition. Also the decreased intensity of the deoxyF^- MCD signal compared to N_3^- may mean a lower pK_a and thus less protonation of the bridge.[53] The behavior with CN^- is more inconsistent, in that it was shown to cause rapid exchange, but is not observed to bind to deoxyHr by CD or MCD. There is no obvious explanation for this, unless CN^- binding and bridge exchange occur in another form of the protein, for example, a transient deoxy species as postulated by Wilkins.[54b]

The oxo–hydroxo equilibrium may also contribute to other aspects of the active site reactivity. DeoxyHr is oxidized to metHr very slowly by one-electron oxidants.[56] However, the two-electron oxidation upon binding of oxygen is rapid.[57] This could result from hydroxide proton transfer to the bound oxygen molecule, resulting in the oxo bridge.[9] During the one-electron oxidation, this proton could remain on the bridging oxygen, slowing the reaction due to either structural constraints or a poor electron exchange pathway. It will be interesting to define the nature of the endogenous bridging ligands in the half-oxidized half-met ($semimet_0$) derivative. In addition, this deprotonation of the bridge may play a role in the structural constraint responsible for the cooperativity in hemerythrin from the brachiopod *L. reevii* which has been shown to have a similar active site structure.

Acknowledgment. This work was supported by NSF Grant DMB-8418294. We thank Prof. Philip Stephens for the use of his IRCD instrument and Profs. Weighardt and Murray for helpful discussions.

Registry No. Iron, 7439-89-6; azide, 14343-69-2; cyanate, 661-20-1; fluoride, 16984-48-8.

Supplementary Material Available: Spectra of MCD, CD, variable-temperature and variable-field MCD, and ground-state energy levels for compounds in the text (4 pages). Ordering information is given on any current masthead page.

(52) In fact Wieghardt has synthesized a binuclear ferrous complex, believed to contain a bis(μ-carboxylato)-μ-aquo bridging system. Private communication.

(53) Note that our results on deoxyX^-Hr, where $X^- = N_3^-$, OCN^-, and F^-, do not necessarily require that the hydroxo bridge is protonated at all sites. The pK_a could be such that an equilibrium exists, with the MCD and EPR being sensitive only to the protonated and thus paramagnetic sites. We can say, however, that the deoxyHr species has essentially no protonated sites at pH 7.7, while the large intensity of MCD and EPR signals indicates a significant percentage of protonated binuclear sites in deoxyN_3^-. It is possible that the appearance of a weaker MCD signal for deoxyF^-Hr could be due to a lower pK_a and thus less of the protonated species present. We are currently quantitating this possibility.

(54) (a) Freier, S. M.; Duff, L. L.; Shriver, D. F.; Klotz, I. M. *Arch. Biochem. Biophys.* **1980**, *205*, 449–463. (b) Bradic, Z.; Conrad, R.; Wilkins, R. G. *J. Biol. Chem.* **1977**, *252*, 6069–6075.

(55) (a) Hunt, H. R.; Taube, H. *J. Am. Chem. Soc.* **1957**, *80*, 2642–2646. (b) Basolo, F.; Pearson, R. B. *Mechanisms of Inorganic Reactions*; Wiley: New York, 1967; pp 165–171.

(56) Bradic, Z.; Harrington, P. C.; Wilkins, R. G.; Yoneda, B. *Biochemistry* **1980**, *19*, 4149–4155.

(57) Bates, G.; Brunori, M.; Amiconi, G.; Antonini, E.; Wyman, J. *Biochemistry* **1968**, *78* 3016–3020.